

See discussions, stats, and author profiles for this publication at: <https://www.researchgate.net/publication/389692683>

FDM – 3D printing of thermoplastic composites with high energetic solids content designed for gun propellants

Article in Defence Technology · March 2025

DOI: 10.1016/j.dt.2025.02.024

CITATIONS

0

READS

93

11 authors, including:



Alexandru Marin

Scientific Research Center for CBRN Defense and Ecology

11 PUBLICATIONS 10 CITATIONS

SEE PROFILE



Ovidiu Iorga

Research and innovation center for CBRN defense and ecology

32 PUBLICATIONS 79 CITATIONS

SEE PROFILE



Gabriela TOADER

Military Technical Academy

67 PUBLICATIONS 460 CITATIONS

SEE PROFILE



Cristiana Epure

Scientific Research Center for CBRN Defense and Ecology

13 PUBLICATIONS 21 CITATIONS

SEE PROFILE



FDM - 3D printing of thermoplastic composites with high energetic solids content designed for gun propellants

Marin Alexandru ^{a, b}, Ovidiu George Iorga ^{a, *}, Gabriela Toader ^{b, **}, Cristiana Epure ^a, Mihail Munteanu ^a, Adrian Nicolae Rotariu ^b, Marius Marmureanu ^c, Gabriel Flavius Noja ^c, Aurel Diacon ^{b, d}, Tudor Viorel Tiganescu ^b, Florin Marian Dirloman ^b

^a Research and Innovation Center for CBRN Defense and Ecology, 225 Olteniței Ave., 041327, Bucharest, Romania

^b Military Technical Academy "Ferdinand I", 39–49 George Cosbuc Boulevard, 050141, Bucharest, Romania

^c Military Equipment and Technologies Research Agency, 16 Aeroportului Street, Clinceni, 077025, Ilfov, Romania

^d Faculty of Chemical Engineering and Biotechnologies, National University of Science and Technology POLITEHNICA Bucharest, 1–7 Gh. Polizu Street, 011061, Bucharest, Romania

ARTICLE INFO

Article history:

Received 14 December 2024

Received in revised form

17 February 2025

Accepted 26 February 2025

Available online xxx

Keywords:

Propellants

FDM

3D-printing

Explosive

RDX

Thermoplastic energetic composite

Additive manufacturing

ABSTRACT

This study represents an important step forward in the domain of additive manufacturing of energetic materials. It presents the successful formulation and fabrication by 3D printing of gun propellants using Fused Deposition Modeling (FDM) technology, highlighting the immense potential of this innovative approach. The use of FDM additive manufacturing technology to print gun propellants is a significant advancement due to its novel application in this field, which has not been previously reported. Through this study, the potential of FDM 3D-printing in the production of high-performance energetic composites is demonstrated, and also a new standard for manufacturability in this field can be established. The thermoplastic composites developed in this study are characterized by a notably high energetic solids content, comprising 70% hexogen (RDX) and 10% nitrocellulose (NC), which surpasses the conventional limit of 60% energetic solids typically achieved in stereolithography and light-curing 3D printing methods. The primary objective of the study was to optimize the formulation, enhance performance, and establish an equilibrium between printability and propellant efficacy. Among the three energetic formulations developed for 3D printing feedstock, only two were suitable for printing via the FDM technique. Notably, the formulation consisting of 70% RDX, 10% NC, and 20% polycaprolactone (PCL) emerged as the most advantageous option for gun propellants, owing to its exceptional processability, ease of printability, and high energetic performance.

© 2025 China Ordnance Society. Publishing services by Elsevier B.V. on behalf of KeAi Communications Co. Ltd. This is an open access article under the CC BY-NC-ND license (<http://creativecommons.org/licenses/by-nc-nd/4.0/>).

1. Introduction

Energetic materials (EMs), covering propellants, explosives, and pyrotechnics, have an essential role across multiple sectors, including defense, aerospace, and commercial pyrotechnics. These materials are specifically designed to release energy via

combustion, deflagration, or detonation, rendering their performance attributes crucial for applications that require high levels of precision and reliability. Recently, there has been an increasing interest in the potential of additive manufacturing (AM) as an innovative approach for the production and design of EMs. Traditionally, EMs were produced using planar-2D techniques such as blade casting, spin coating, inkjet printing, and electrochemical or vapor deposition [1]. Nevertheless, recent advancements have expanded the possibilities of volumetric-3D methods, including direct writing [2], fused deposition modeling (FDM) [3–5], photopolymerization [6–8], Volumetric Additive Manufacturing (VAM) [9], and binder jet [10,11]. These techniques offer precise control,

* Corresponding author.

** Corresponding author.

E-mail addresses: ovidiu.iorga@nbce.ro (O.G. Iorga), nitagabriela.t@gmail.com (G. Toader).

Peer review under the responsibility of China Ordnance Society.

<https://doi.org/10.1016/j.dt.2025.02.024>

2214-9147/© 2025 China Ordnance Society. Publishing services by Elsevier B.V. on behalf of KeAi Communications Co. Ltd. This is an open access article under the CC BY-NC-ND license (<http://creativecommons.org/licenses/by-nc-nd/4.0/>).

enabling the manufacture of energetic structures with enhanced characteristics. The performance of EMs depends on several factors, including their composition, structure, and processing techniques. The method used for shaping the EMs is particularly critical, as it influences both scalability and safe processing [12].

Current research has explored various 3D printing methods tailored for energetic materials [13,14]. The technique of photopolymerization is commonly utilized in the 3D printing of energetic materials due to its capability to provide precise control over the placement of materials and facilitate layer-by-layer construction. By selectively curing liquid resin through exposure to light, it is possible to construct complex structures with high resolution and reduced waste. This process was formerly called "Stereolithography" (SLA) [7,15,16]. This approach is especially beneficial for the fabrication of custom-shaped energetic components, including EMs, while ensuring both safety and precision. Straathof et al. [7] used light-curing 3D printing technology to print gun propellant grains based on RDX (hexahydro-1,3,5-trinitro-1,3,5-triazine, 50 wt%), acrylate binders (~24 wt%), and energetic plasticizer (~24 wt%). The authors concluded that further investigation is necessary to increase the energetic content and that FDM printing would be a more advantageous option. Yang et al. [6] used the same technique (SLA) to print gun propellant grains composed of RDX (50 wt%), epoxy acrylate derivative (25 wt%), Bu-NENA (N-n-butyl-N-(2-nitroxyethyl) nitramine, 12.5 wt%), reactive diluent and additives (12.5 wt%). When ignited within a closed bomb, both propellants exhibited a high pressure exponent, attributed to the porosity of the material. Additionally, probably due to the reduced RDX content in the formulation, they yielded comparatively low energy output. Experimental firings using a 30 mm muzzle revealed incomplete combustion of both propellant formulations [6,7]. Li et al. [8] designed a CL20 (Hexanitrohexaazaisowurtzitane Dodecane, 60 wt%), Bu-NENA (10 wt%), and APNIMMO (acrylate-terminated poly-3-nitratomethyl-3-methyl oxetane oligomer, 30 wt%) formulation for SLA printing. They reported a better linear burning rate and specific energy $f(\text{force})$ of 996 J/g, compared to the 870 J/g value reported for composition developed by Straathof et al. [7].

An alternative 3D printing method known as "direct writing" involves the precise deposition of a "reactive ink" onto a substrate. The structures formed through this technique solidify due to solvent evaporation or binder precipitation, leading to the generation of self-supporting specimens. By using this technique, an energetic CL-20-based slurry incorporating 29–31 wt% solvent was used for loading holes in micro-electric initiators for micro-electromechanical system (MEMS) used as safe and arm (S&A) devices [17]. This direct writing technique implied incorporating CL-20 into an aqueous volatile mobile phase and also into a non-aqueous volatile mobile phase. The two phases were subsequently mixed and introduced into the microelectromechanical systems (MEMS) device, where the solvents evaporated, depositing the high explosive. The application of the solvent-based slurry occurred in successive layers, with the addition of each new layer depending upon the complete evaporation of the solvent from the preceding layer [18]. Nonetheless, the viscosity of the materials presents considerable challenges, making it difficult to achieve high energetic loading.

Gao et al. [18] printed photocurable gun propellants via 3D material extrusion technology, using a polyurethane-acrylic acid resin as a binder and CL-20 as an energetic filler at 70 wt%, 75 wt%, and 80 wt% concentrations. The force constants they obtained ranged from 1107.43 to 1209.44 J/g, but they affirmed that further optimization of CL-20-based photocurable formulations is necessary to reduce the pressure exponent. Wang et al. [19] investigated 3D printing of conventional double-based gun propellant (NC

58.5 wt%, NG 40 wt%, centralite 1 wt%, vaseline 0.5 wt%) using the laminated object manufacturing (LOM) technique. The LOM approach employs a "cut-then-bond" method, which involves mechanically cutting propellant sheets and then bonding them layer by layer with adhesive, allowing for complex geometrical designs. Ethyl acetate served as a layer-to-layer adhesive due to its proper solubility for gun propellants and its high volatility.

The FDM printing technology has been reviewed by Muravyev [1] and Kudryashova [20], mainly focusing on nanothermites, fluoropolymers, or HTPB-AP (hydroxyl-terminated polybutadiene - ammonium perchlorate). However, to the best of our knowledge and based on the existing literature, the successful 3D printing of gun propellants containing high explosives has not yet been accomplished using Fused Deposition Modeling (FDM). This limitation can be attributed to the inherent thermolability of the components commonly employed in propellant formulations and to the challenges created by the high solid content and increased viscosity. With higher solid loading in propellant formulations, commercially available adhesives and binders designed with single-curing functionalities like photocuring or thermocuring prove inadequate [12] to satisfy the 3D printing requirements of gun propellants. Consequently, the development of innovative formulations and technical solutions tailored specifically for FDM-based 3D printing of gun propellants represents a frontier filled with both remarkable opportunities and numerous obstacles.

The process of additive manufacturing for EMs through Fused Deposition Modeling (FDM) requires a careful balance between enhancing performance and recognizing inherent constraints. Essential factors to consider include the modification of particle size distribution, the formulation of binder composition, and the management of rheological properties. Adjusting these parameters significantly affects the flow behavior of the material and its ignition characteristics. Moreover, it is essential to maintain strict temperature control during the printing process, as excessive heat can lead to the degradation or premature reactions of the energetic materials. Additionally, the optimization of nozzle geometry plays a crucial role in the accuracy of layer deposition. Achieving an appropriate balance between layer height and printing speed is vital for ensuring both resolution and efficiency. Notably, the integration of materials with differing viscosities within a single print can effectively address challenges, enabling the creation of complex geometries while maintaining overall performance.

Polymers employed as binders and/or as plasticizers play an essential role in gun propellants by improving their processability while ensuring cohesion between the components and optimal mechanical properties. Some examples of such polymeric matrices employed for this purpose include: Hydroxy-Terminated Poly-Butadiene (HTPB), Nitrocellulose (NC), Glycidyl Azide Polymer (GAP), Poly(Glycidyl Nitrate) (PolyGLYN), Triethylene Glycol Dinitrate (TEGDN).

Another promising polymeric candidate for this type of application is polycaprolactone (PCL) [21]. PCL is widely used in 3D printing technology, especially in biomedical applications, because it is a biocompatible and biodegradable material [22]. Arif et al. [23] and Yang et al. [24] have reported that composite PCL-based polymers have good printability and mechanical properties, being able to incorporate high amounts of ceramic and metallic powders. PCL was employed to encapsulate a TNT and an RDX simulant with the aim of formulating an energetic material suitable for application in SLS (selective laser sintering) additive manufacturing, as detailed by Jiba et al. [25]. They concluded that even if PCL can be successfully used for coating RDX and TNT, the SLS 3D printing technology is not recommended for this type of material as the temperature developed during printing could cause the auto-ignition of the energetic material. The chemical compatibility and

thermal properties of RDX-PCL and RDX-AN (ammonium nitrate)-PCL compositions were studied by Haung et al. [26]. They employed VST (vacuum stability tests), TGA (thermogravimetric analysis), and DTA (differential thermal analysis) and concluded that PCL-RDX compositions are chemically stable and the decomposition temperature of RDX is not influenced by the presence of PCL.

In the current era, it is imperative to strike a careful balance between innovation and responsible application. The utilization of 3D-printed gun propellants presents a promising avenue for enhanced safety, supported by their precise geometric configuration and controlled composition. This method offers an effective means of mitigating the inherent risks associated with conventional manufacturing practices while maintaining high ballistic performance standards.

When developing a propellant, it is important to carefully consider its combustion characteristics. It is highly desirable that the combustion process yields a significant quantity of low molecular weight gaseous products along with a substantial amount of heat. This is crucial for maximizing the pressure within the gun barrel and ultimately enhancing the propellant's effectiveness. Based on existing information, FDM printing has not been utilized in the additive manufacturing of gun propellants in the past. Furthermore, according to the literature, although propellant formulations utilized in 3D printing with light-curing techniques have achieved energetic solids loading of up to 80wt% energetic content [18,27], this level of energetic concentration has not yet been realized with the FDM 3D-printing method.

The main issue being addressed in this study is the challenge of formulating and fabricating gun propellants using Fused Deposition Modeling (FDM) technology, which has not been previously reported in this field. To effectively address the challenges associated with producing gun propellants using Fused Deposition Modeling (FDM) technology, we optimized and characterized thermoplastic energetic composite formulations specifically designed for FDM printing. This process involved refining material ratios and processing parameters to improve mechanical and thermal properties, ensuring optimal performance. We conducted comprehensive testing to evaluate the performance and safety of the formulations. Our goal was to develop reliable and efficient FDM-printed gun propellants that adhere to industry standards.

Thus, this study presents the implementation of an RDX-nitrocellulose (NC)-polycaprolactone (PCL) formulation for gun propellants 3D printing by FDM additive manufacturing technology, more specifically through fused granulate fabrication (FGF). The objective was to achieve a minimum of 60% high explosive solid content in the propellant. RDX was selected as it is used frequently in composite gun propellants and is also available in bulk quantity, while PCL was chosen due to its low melting point, which is essential to avoid the autoignition of the energetic components RDX and NC. The incorporation of NC is intended to enhance the mechanical properties of the propellant composite and to offer a supplementary energy contribution, thereby improving the overall quality and performance of the 3D printed materials. We developed three formulations, two of which were suitable for FDM printing. The leading formulation, made up of 70% RDX, 10% nitrocellulose, and 20% polycaprolactone (PCL), showcased remarkable processability, printability, energetic performance, and safety. The innovative aspects of this study demonstrate the potential of FDM 3D printing in producing high-performance energetic composites, establishing a new standard for manufacturability in this field. The successful integration of high explosive content (RDX and NC) in FDM-printed propellants represents a significant advancement; thereby, the article explores the development of formulations and processing parameters to optimize 3D printing using the FDM

approach, focusing on gun propellants containing 80% energetic components by weight.

2. Materials and methods

2.1. Materials

The cyclotrimethylenetrinitramine/hexogen (**RDX**, 1.82 g/cm³ crystal density, melting point >200 °C, purity >95%), conforming to MIL-DTL-398D, type I, class I, was acquired from energetic materials factory "Fabrica de pulberi Făgăraș" Romania as unphlegmatized crystals (15wt% water content). The nitrocellulose (**NC**, white fibrous solid, 12.6% nitrogen content, autoignition temperature >180 °C, 30 wt% butanol content) was acquired from "Milan Blagojevic-Namenska" energetic materials factory, Serbia. The polycaprolactone (**PCL**, ≈3 mm beads, 99.5% purity, average molecular weight $M_n = 80000$ Da, 1.145 g/cm³ density) was purchased from Sigma Aldrich. The solvents: dichloromethane (**DCM**, 1.3 g/cm³ density, 99.5% min. purity), acetonitrile (**ACN**, 0.79 g/cm³ density, 99.5% min. purity), and n-Hexane (0.66 g/cm³ density, min. 99.7% purity) were obtained from Merck and were used as received. Double-distilled water was utilized for the formulations.

2.2. Methods

2.2.1. Preparation of the materials

2.2.1.1. Formulating the energetic composite grains necessary for the extrusion process. The RDX and the NC were dried for 48 h in a ventilated oven at 60 °C to remove moisture and alcohol content, respectively. Subsequently, the RDX was separated through a 90 μm opening ASTM No. 170 sieve, and only the passing fraction was further used. The NC was dissolved in ACN (1:4, w/w), at 20 °C, by magnetic stirring for 4 h. The PCL was dissolved in DCM (1:4, w/w), at 20 °C, by manual stirring with a glass rod. The composition of the formulations intended for use in grain form for FDM printing is detailed in Table 1 below.

The formulations outlined in Table 1 were produced by blending the NC solution with the PCL solution in appropriate ratios. Following this, the RDX powder was added, and the resulting slurry was manually mixed. The shock-gel procedure (Fig. S1, supporting info file) was further applied to eliminate the solvent. The slurry was poured into an n-hexane-filled beaker (1:4, w/w) and was vigorously stirred (mechanically stirring, 300 rpm, 4-blade anchor stainless-steel mixer) until the slurry started to separate into suspended particles. Subsequently, the liquid phase was discarded, and a fresh quantity of n-hexane was added to the energetic grains (4:1, w/w), followed by further stirring. This procedure was repeated twice for each energetic formulation containing RDX, NC, and PCL. Solid particles settled at the bottom of the beaker after stirring stopped. The material was then filtered from the liquid phase and dried for 24 h at 40 °C in a ventilated oven. The PCL-RDX slurry (sample code HNP 800020) was produced by incorporating RDX powder directly into the PCL solution. The PCL-RDX slurry (100 g) was slowly poured into a beaker containing 500 mL of double-distilled water at 35–37 °C while vigorously stirring (mechanical stirring, 300 rpm, 4-blade stainless-steel mixer), causing the slurry to form suspended grains. The stirring process was

Table 1
Composition of the energetic formulations.

Sample code	RDX/wt%	NC/wt	PCL/wt
HNP 570736	57	7	36
HNP 701020	70	10	20
HNP 800020	80	0	20

extended for 2 min, and subsequently, an additional 200 mL of cool water at 15 °C was gently introduced into the beaker while continuing to stir for an additional 2–3 min until the suspended particles started to adhere to beaker walls. The resultant grains were separated from the water and subsequently subjected to a 48-h drying process at 40 °C in a ventilated oven. Figs. S1(b) and S1(c) from the supporting info file exemplify the aspect of the grains obtained after the drying process.

2.2.1.2. Preparation of the extruded filaments serving as granulate feedstock for FDM printing of gun propellants. A hot press extrusion process, followed by cutting the extruded filaments to a 3 mm length, was implemented to obtain the granulate feedstock for 3D printing of gun propellants. Prior to the extrusion process, the grains obtained from the shock-gel procedure and the extrusion device were placed in an oven and heated together at 110 °C for 2 h. Afterward, the material was extruded at 110 °C and 37 MPa pressure in a continuous filament through a 1.5 mm opening (Fig. S2, supporting info file).

2.2.2. FDM printing of gun propellants

For this step, a commercial 3D printer system, Pico Creat G5Pro FGF, was employed. The successful operation of the 3D printer system requires the secure installation of the printer on a stable, level surface to minimize vibrations. Initially, a CAD file describing the desired geometry of the object to be materialized through printing was created. Subsequently, the file underwent pre-processing using the dedicated software "Creality Print". The formulations used for printing incorporate a brisant explosive (RDX) as the primary energetic constituent (57–80 wt%), with a self-ignition temperature of 219 °C (according to AOP-4491 "Energetic Materials Thermal Sensitiveness and Explosiveness Tests" standard). As binder, an inert polymer (PCL) with a melting temperature of ~60 °C and a relatively stable energetic binder (NC) capable of maintaining thermal stability up to 170 °C were used. Consequently, the printing temperature was calibrated to 150 °C to align with the flow characteristics of the energetic formulation while remaining safe for operation. The platform was preheated to a temperature of 80 °C to control the adhesion of the initial layer. Subsequently, a commercial glue, mainly based on polyvinyl acetate, served as print bed adhesive layer. A proper bonding between melted material layers requires a gradual cooling process. The Pico Creat G5Pro FGF 3D printer is equipped with a cooling system featuring a dual-opening fan symmetrically positioned around the printing nozzle. However, in our case, the fan was entirely deactivated by adjusting the control button to the "0" scale while the ambient temperature was kept at 20 °C. The combined operation of the fan with an ambient temperature of 20 °C. Through iterative trials, efforts were focused on establishing a flow rate set at 200%, setting the material layer width equal to the diameter of the printing nozzle, and fixing the material layer height at 0.2 mm. Printing speeds were configured at 15 mm/s for both the exterior walls and infill, enabling the creation of homogeneous structures with material layers adhering effectively to one another. Additionally, to ensure a robust connection between the deposited layers forming the walls and those utilized for infill, a 40% overlap between them was established based on the infill layer width. These technical adjustments played a fundamental role in achieving cohesive and high-quality energetic 3D printed structures suitable for use as gun propellants.

2.3. Characterization

Prior to formulating energetic composites, a theoretical assessment was conducted to determine the optimal composition of gun

propellants using EXPLO5™ (version 6.05), a computer program developed by M. Suceasca [28]. The software serves as a versatile tool for predicting the energetic properties and calculating detonation parameters of explosives. It has the capability to forecast the detonation properties of both new individual explosives and various energetic composites. The implementation of the modeling stage prior to the experimental phases in this study aim to leverage the powerful capabilities of EXPLO5™ to streamline the experimental process and to minimize the need for supplementary, potentially hazardous experiments. Therefore, the thermodynamic and chemical equilibrium was theoretically calculated using a numerical method. In order to simulate the conditions encountered in closed bomb testing, an isochoric combustion model was implemented with the following assumptions: 1) The chemical equilibrium, at a given temperature and pressure state, is described by a system of equations based on the minimization of free energy method and is solved by the Newton-Raphson method; 2) Third term virial equation is used to describe the thermodynamic state of gaseous combustion products and to calculate the pressure inside the vessel; 3) The condensed combustion products (if any) are considered incompressible and their thermodynamic functions in their standard state are derived from the enthalpy, as a function of temperature by the fourth-degree polynomial. Reactant thermochemical data is presented in Table S1 from the supporting info file.

The morphology investigation of the obtained gun propellants was performed by SEM analysis of the gun propellants using a Tescan Clara model S8152, in high-vacuum mode, 1 kV acceleration voltage, in wide-field and resolution mode using a secondary electron (SE) detector. The specimens were carefully mounted on aluminum stubs using carbon tape and subsequently coated with a fine layer of gold through the sputtering process. The sputtering process was performed in an argon atmosphere at 2 kV for 3 min.

FTIR analysis was carried out using the PerkinElmer Spectrum Two FT-IR Spectrometer equipped with MIRacle™ Single Reflection A.T.R. from PIKE Technologies, setting the following parameters: transmission mode scanning, 32 scans, 4 cm⁻¹ resolution.

The mechanical properties of the 3D printed energetic composites were investigated on a Discovery 850 DMA analyzer from TA Instruments in four different types of setups: single cantilever scan on temperature ramp (single cantilever loading under periodic stress for investigating storage modulus, loss modulus, and tan delta), shear-sandwich setup (for the evaluation of the frequency-dependent shear modulus), tensile test setup (using a tensile clamp, designed for uniaxial deformation investigations), and 3-point bending setup (to evaluate the flexural properties).

For the temperature scan, we utilized a 17.5 mm single cantilever clamp for testing samples measuring 36 mm × 12 mm × 3 mm. The temperature increased from -80 °C to 40 °C with a ramp rate of 5 °C/min, while maintaining a constant frequency of 1 Hz and an oscillation amplitude of 20 μm.

Using the shear sandwich setup on the same instrument, two equal-size square-shaped slices of the same material (12 mm × 12 mm × 2 mm) were sheared between two fixed plates and a moving plate to evaluate the shear modulus. To ensure good adherence between the samples and the clamps in shear sandwich mode, a compressive pre-strain of 1% was applied to the 3D-printed specimens. The test was performed at 25 °C and the frequency was logarithmically increased from 10⁻¹–10² Hz.

After installing tensile clamps on the Discovery 850 DMA analyzer, tensile tests were conducted on rectangular samples, at a constant temperature of 25 °C. The tensile properties of the HNP702010 propellant were measured using a group of 5 samples of parallelepipedal shape, having 30 mm length, 8 mm width, and 1 mm thickness. The printing was performed in only one orientation (parallel pattern, lines), parallel with the vector of applied

tension, using a layer height of 0.2 mm, and a layer width of 0.8 mm with an overlap of 40%. The tests were conducted at a speed of 1 mm/min with a preload force of 0.1 N.

The three-point bending test was carried out on the same Discovery 850 DMA using dedicated 3-point bending clamps in oscillation mode. The samples underwent a three-point bending test at 25 °C in oscillation strain-sweep mode (sweep mode - logarithmic), using a preload force of 0.1 N. During the conducted test, the amplitude was varied within the range of 1–500 μm , while maintaining a constant frequency of 10 Hz. The 3-point bending analysis was conducted in triplicate for each type of 3D-printed material.

Mechanical characterization was completed with a series of quasi-static and dynamic uniaxial compression tests at room temperature on hexahedron small materials specimens (10 mm \times 10 mm \times 7.5 mm) cut from the printed samples. The quasistatic tests were performed with Titan 10 universal testing machine and in the dynamic tests was used a flat end projectile of 0.65 kg, horizontally propelled by a compressed air cannon with impact velocities between 3.5 and 5.5 m/s against a propellant specimen placed on a flat surface fixed target. To acquire relevant data in the dynamic tests, a PCB 350C03 accelerometer was attached to the base of the projectile, and a PHOTRON SAZ high-speed camera was used to record images. The specimens were positioned so that the compression, both in the static and dynamic tests, was carried out on the growth axis of the propellant samples during 3D printing.

To investigate the thermal properties of the energetic composites obtained by FDM printing was performed by DSC analysis using a PerkinElmer Diamond 8000, with a heating ramp rate of 10 °C/min. The low-temperature analysis (melting survey) was performed in aluminum crucibles, using samples weighing approximately 10–12 mg. The high-temperature DSC analysis (degradation-autoignition survey) was performed on 1–2 mg of sample loaded in a high-pressure steel crucible. Also, heat flow calorimetry (HFC) analysis was performed on a TAM IV heat flow microcalorimeter from TA Instruments, in isothermal mode, at 90 °C for 100 h, for 1 g of samples loaded in sealed 4 mL ampules, as described by NATO STANAG 4582- *Explosives, nitrocellulose-based propellants, stability test procedure and requirements using heat flow calorimetry* [29].

Impact sensitivity was tested with a BAM fall hammer BFH12 manufactured by OZM Research. The tests were performed according to NATO STANAG 4489 - *Explosive, impact sensitivity test* [30].

Friction sensitivity tests were performed with a BAM friction apparatus FKSM 10 from OZM Research, in accordance with the method described in NATO STANAG 4487- *Explosive, friction sensitivity test* [31].

Closed bomb testing was conducted to evaluate the performances of the developed energetic formulations. Closed bomb testing was performed in a 40 cm³ OZM TSV closed vessel. The ballistic evaluation was performed at three load densities related to the volume of the combustion chamber: $\Delta_1 = 100 \text{ kg/m}^3$, $\Delta_2 = 150 \text{ kg/m}^3$, and $\Delta_3 = 200 \text{ kg/m}^3$. To initiate the ignition of the propellant charges, an electric pyrotechnic igniter was employed along with a small quantity of black powder, constituting 10 wt% of the propellant tested. In addition, testing was conducted on the ignition system (pyrotechnic igniter and black powder), and the pressure-time profile was subtracted from the recorded data of the tested propellant. A schematic drawing of the instrumental setup and the closed bomb is shown in Fig. S3 from the *supporting info file*. The closed bomb tests performed were complemented by the use of EXPLO5™ simulations as a versatile tool for predicting energetic properties and providing a comprehensive overview of the propellants developed.

3. Results and discussion

3.1. Explo5™ - based considerations for the design of the 3D-printed gun propellants

As outlined in the *Characterization section*, a modeling stage was used to minimize potential risks associated with experimental procedures to establish efficient propellant formulation. The calculations were conducted using EXPLO5™ to analyze the influence of the various proportions between the components RDX-NC-PCL in the HNP (H – hexogen = RDX; N – nitrocellulose; P – polycaprolactone) formulations. The results are documented in Table S2 from the *supporting information file*. Subsequently, ballistic energy (propellant force, F), heat of combustion (Q_c), and adiabatic combustion temperature (T_c) were represented on a ternary graph based on composition, as depicted in Fig. 1.

The ballistic performance of a propellant is commonly expressed as specific energy (propellant force), $F = n \times R \times T$ (MJ/kg) where n is the number of gas moles of combustion products/kg of propellant, R is the gas constant of combustion products, and T is the flame temperature of combustion products. When utilizing propellant in a gun barrel, it is important to ensure that it does not undergo detonation or generate solid residue or corrosive combustion products. Neglecting this principle may lead to detrimental effects on the firearm and endanger the safety of the operator. Excessive temperatures generated during combustion can significantly impact the lifespan of a firearm barrel. To optimize safety and longevity, it is preferable to maximize propellant force using the n factor rather than the T factor.

Since the objective of this research was to find the right combination of components to include a minimum of 60 wt% high explosive in the gun propellant formulations, we employed EXPLO5™ to refine various composition adjustments until we achieved the desired balance of optimal performance and processability suitable for FDM printing. The EXPLO5™ evaluation process began by examining the performance of the formulation labeled HNP800020. The findings indicated that it had the potential to achieve high ballistic performance due to its high specific energy and heat of combustion (see Fig. 1 and Table S2). However, concerns arose regarding the high solid content and its potential challenges during the extrusion process. To address this, 10 wt% of the high explosive (RDX) was replaced with an energetic binder (NC), resulting in the formulation named HNP701020.

Subsequently, we compared the performance of HNP800020 and HNP701020 with a composition featuring a higher polymeric content labeled HNP570736. It was determined that higher PCL content was not suitable for this type of application, as it would result in lower performance values (see Fig. 1 above and Table S2 from the *supporting info file*). Based on the EXPLO5™ assessment, it has been determined that all three selected formulations can constitute favorable solutions upholding high energetic performance (see Fig. 1 above and Table S2 from the *supporting info file*), thus the next step consisted in demonstration of the feasibility of the fabrication by FDM technique.

3.2. Optimizing FDM printing of gun propellants

To produce the granulate feedstock for FDM printing of gun propellants, a hot press extrusion process was employed to create filaments, which were later trimmed to a length of 3 mm. The procedure is detailed in the *Methods section*. The resulting filaments (Figs. S4(a) and S4(b)) were cut using a steel cutter and a patterned 3D-printed board (Fig. S4(c)). The aspect of the granules obtained is exemplified in Fig. S4(d). As can be observed from Fig. S4(a), for the HNP800020 propellant formulation, the resulting filaments

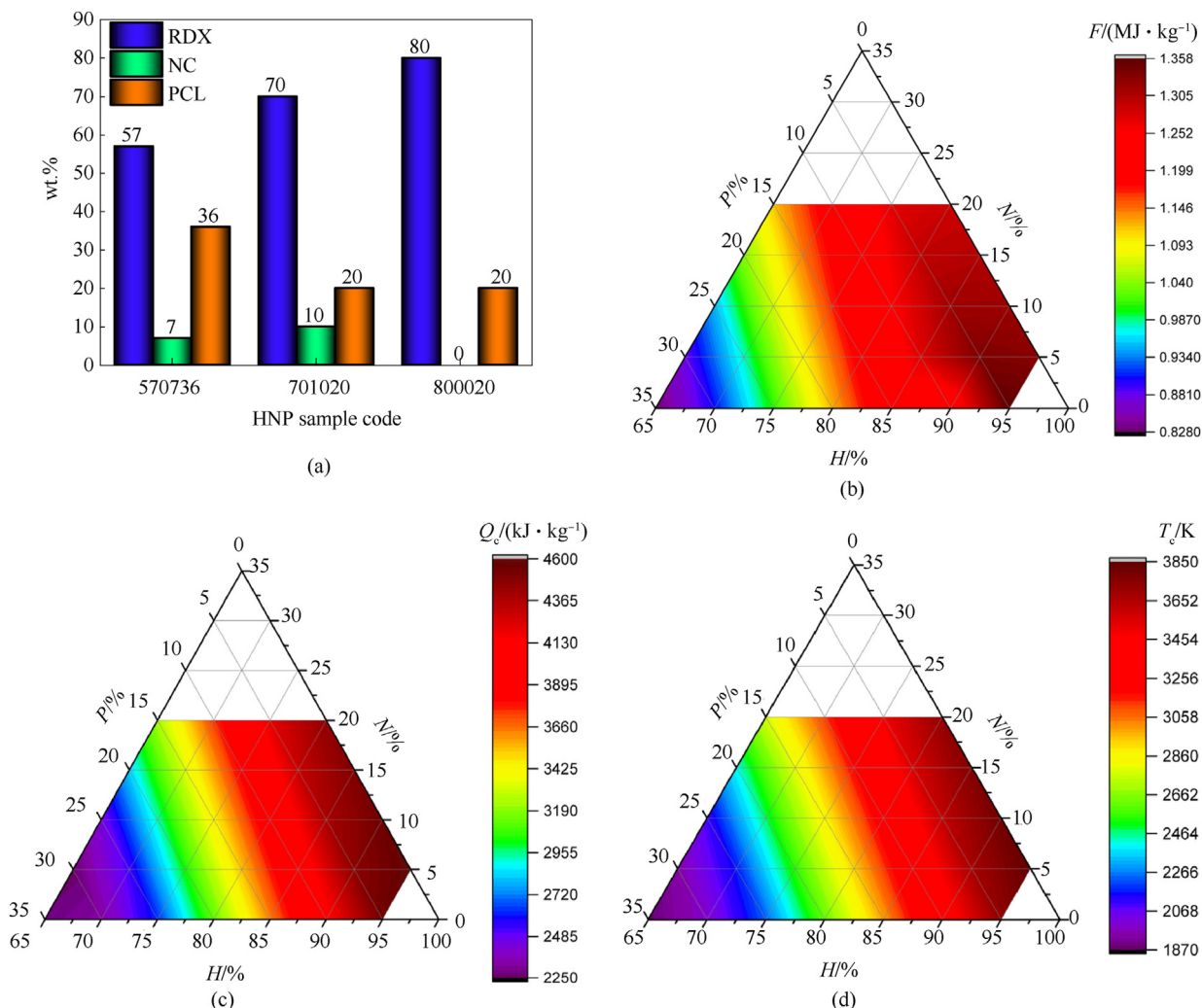


Fig. 1. Ternary graphs, based on EXPL05™ results, describing the influence of the components on the properties of the propellants HNP formulations (**H**-RDX, **N**-NC, **P**-PCL): (a) wt% composition of the HNP formulations employed in the study; (b) Specific energy (propellant force); (c) Heat of combustion; (d) Adiabatic combustion temperature.

displayed a lack of surface continuity, featuring numerous defects, with RDX crystals prominently protruding from the polymer matrix. In contrast, the HNP701020 propellant formulation shown in Figs. S4(b)-S4(d) demonstrated excellent processability, displaying a consistently smooth continuous surface, optimal incorporation of the RDX crystals within the PCL-NC blended matrix, and overall improved compatibility among the components. The formulations presented in Table 1 and Fig. 1(a) have been fabricated in 300 g batches. Successful printing was only achieved for two out of the three formulations (HNP570736 and HNP701020). These two formulations were the only ones that allowed for a qualitative extrusion into $\varnothing 1.5$ mm filaments, which were then cut into 3 mm long granules. In contrast, due to the lack of processability demonstrated in the extrusion process, HNP800020 was deemed suitable for use as a propellant in its original spherical shape, directly as it was obtained through the shock-gel process. The illustration below (Figs. 2(a) and 2(d)) depicts the FDM printing process of HNP570736 and 702010 using Piocreate G5Pro FGF printer and the resulting materials.

The printing process for both compositions was carried out using the same procedure and configuration parameters. No significant issues were encountered during the printing of these materials. Nonetheless, a few minor challenges were noted, which are outlined below. The flow properties of the mixture, along with the constraints

of the 3D printer and the minimum nozzle diameter of 0.8 mm, posed some challenges in achieving high-resolution prints. This was particularly evident with complex geometries that required fine details. However, these factors provide valuable insights into future improvements in the printing process. One additional concern observed pertains to the blockage of the extruder feed that occurs between consecutive print sessions. This blockage is the result of the material within the extruder cooling completely. At the end of the initial print session, the pellets in the upper section of the extruder melt, and upon cooling, they form a solid mass that resembles a gum-like conglomerate. Addressing this issue is crucial for maintaining optimal printer performance. When initiating a new print session, insufficient heat transfer to the upper section of the extruder prevented the material from remelting properly, resulting in a blockage of the feed mechanism. This issue was addressed through manual intervention, using tweezers to carefully maneuver the material into the grooves of the feed screw.

3.3. Investigation of the 3D-printed gun propellants morphology

The morphological characteristics of the extruded filaments employed as granulate feedstock for FDM printing of gun propellants, along with those of the 3D-printed specimens, were subject to evaluation through SEM analysis. The results for

HNP701020 extruded filament and 3D printed gun propellant are presented in Fig. 3, while for HNP570736 and HNP802020, the SEM images for the extruded filament and the corresponding 3D printed gun propellant are presented in Figs. S5 and S6 respectively.

SEM investigation of the three types of extruded filaments revealed that the HNP 701020 filament (Fig. 3(a)) displayed lower rugosity in comparison to HNP 570736 (Fig. S5(a)) and HNP800020 (Fig. S6) which can be attributed to an optimal NC content.

Fig. 3(a) shows that the HNP701020 filament features a polymer blend film on its exterior wall, with no RDX crystal protruding from the film. Moreover, the sectioned filament displays a balanced distribution of RDX crystals within the polymer blend. This balanced distribution could prove advantageous for safely printing the propellant grains, resulting in an expected decrease in friction sensitivity. In the case of HNP570736 (Fig. S5), the material appears uniform both on the exterior surface and in the cross-section view. The lower RDX quantity (57 wt% in the case of HNP570736, compared to 80 wt% in sample HNP701020) leads to a slightly distinct morphology. Specifically, the RDX crystals are only sparsely observable, most likely due to better coverage by the polymeric blend. Nevertheless, probably due to less reinforcement provided by fewer RDX crystals, the HNP570736 filaments present some defects on their outer surface. Fig. S6 illustrates the morphology of the filament extrusion attempt for HNP800020. The filament exhibits noticeable breaks, collars, and irregularities, while the RDX crystals seem to be detached from the surrounding material (PCL).

The morphology of the 3D-printed specimens HNP701020 and HNP570736 was further evaluated, and the relevant SEM images are shown in Fig. 3(b) and Fig. S5(b), respectively. The surface of the 3D-printed HNP701020 specimen displays a network of coated RDX crystals and voids. Due to the presence of RDX crystals and voids on its surface, this material is anticipated to ignite more readily than the HNP701020 in its extruded filament form. In contrast, the SEM survey on the surface of the 3D-printed HNP570736 specimen revealed a continuous matrix of polymer blend fully covering the RDX crystals, with no observable voids on the printed surface. In the context of comparison, Fig. S6(a) illustrates SEM images of the grain structure of the HNP800020 sample, as it was not feasible to 3D-print this material. SEM imaging revealed numerous voids on both the surface and within the material (cross-section view). It was observed that the RDX crystals did not adhere to the PCL matrix but rather seemed to be physically trapped within the polymeric matrix. This phenomenon of void formation is likely due to the generation of dichloromethane vapors inside the grain during the drying phase of HNP800020 preparation.

3.4. Physicochemical characteristics of the 3D printed gun propellants

FT-IR spectroscopy was utilized to investigate the chemical composition and structure of the 3D-printed gun propellants, and the results are presented in Fig. 4 and Fig. S7. The first peak from the CH stretching region of the FT-IR spectra at 3074 cm^{-1} could be assigned to the CH stretching of the nitramine. The following absorption band observed at 2951 cm^{-1} is ascribed to the asymmetric stretching of C-H hydroxyl groups in PCL. The carbonyl stretching in PCL is visible at 1724 cm^{-1} . The peaks at 1590 and 1386 cm^{-1} can be assigned to the N-O asymmetric stretch and N-O symmetric stretch, respectively. C-N vibrations can be associated with the peak at 908 cm^{-1} . The stretching and twisting vibration absorption peaks of O-NO₂ are observed at 842 , 752 , and 671 cm^{-1} , respectively.

The chemical stability of the formulations was evaluated according to the criteria specified in NATO STANAG 4582- *Explosives, nitrocellulose-based propellants, stability test procedure, and*

requirements using heat flow calorimetry, respectively, the energetic material should not generate an exothermic heat flow higher than $350\text{ }\mu\text{W/g}$ for 3.43 days. For comparison, the same test was performed on a spherical NC-based propellant (SP) containing 90% NC, stabilized with DPA (diphenylamine). The results of the HFC test for assessing the chemical stability of HNP formulations are illustrated in Fig. S8(a), and it can be observed that the registered values fall within the limitations of the NATO standard mentioned [29], confirming the chemical stability of the tested formulations. The results are illustrated in Fig. S8(b) and Table S3 from the *supporting info file*. The chemical compatibility of the ingredients used in the formulation of HNP was evaluated in accordance with the criteria stated in NATO STANAG 4147 - *Energetic materials, chemical compatibility with munition components* [32,33], as indicated in Eq. (1) described below:

$$Q_R = Q_M - Q_{M,calc} = Q_M - \frac{m_E \cdot Q_E + m_C \cdot Q_C}{m_E + m_C} \quad (1)$$

The absolute increase in the heat generation of the mixture of energetic material and test material, compared to the heat generation of the components separately, is calculated according to Eq. (1), where Q_C = energy release of contact material until t (J/g); Q_E = energy release of energetic material until t (J/g); Q_M = energy release of mixture until t (J/g); $Q_{M,calc}$ = calculated energy release of mixture until t (J/g); Q_R = energy release of inter-reaction until t (J/g); m_C = mass of contact material in the mixture (g); m_E = mass of energetic material in the mixture (g). According to AOP-4147 [32], if Q_R exceeds 30 J/g (approximately 1% of a propellant's heat of decomposition) within t then the test material must be considered incompatible with the propellant. Conversely, if it is below 30 J/g it can be considered as being compatible. The results that refer to the chemical compatibility of the gun propellant components, in accordance with STANAG 4147, are presented in Table S4 of the *supporting information file*.

The findings indicate that the predominant heat-generating substance is NC, with the reaction attributed to the autocatalytic de-nitration of cellulose in the absence of a chemical stabilizer. It is noteworthy, however, that the measured signal falls considerably below the anticipated heat flow calculated by Eq. (1). The observed phenomenon can be attributed to the fact that the individual HNPs were loaded into the ampules in granular form and subsequently reacted with the oxygen present in the air trapped within the ampule [29]. Both chemical compatibility and stability tests indicate that the HNP formulations are sufficiently stable to be stored, handled, and used for at least 10 years.

3.5. Thermal properties of the HNP propellants

To conduct a comprehensive assessment of the thermal properties of the HNP formulations, an extensive differential scanning calorimetry (DSC) analysis that encompassed a wide range of parameters and conditions was performed.

The first stage of the DSC analysis series involved examining various combinations of PCL-NC blends to systematically investigate the influence of the relative proportions of the components on the thermal characteristics of the blends, and the results are illustrated in Figs. S9 and S10.

As can be observed from Fig. S9, in PCL-NC blends where the PCL amount exceeds that of NC by double or more, a clear melting peak is observed. Conversely, in blends with a higher proportion of NC, the melting peak is no longer visible. When PCL is mixed with NC, the DSC melting peak typically shifts to lower temperatures and becomes broader until it is no longer visible. Moreover, during the reheating cycle, at higher NC content, the blends failed to reform

PCL crystallinity, indicating the presence of multiple amorphous phases [34].

Another series of DSC analyses was undertaken to investigate the glass transition of the PCL:NC blends. The results have been detailed in Fig. S10 and Table 2.

Blends are the result of physically combining two or more polymers, and the primary interaction between their segments is intermolecular, leading to the formation of either miscible or immiscible blends. Consequently, the glass transition temperature (T_g) is commonly utilized to gauge the miscibility between polymers and is an indispensable tool for characterizing blends [35]. As can be observed from Fig. S10 and Table 2, PCL possesses a negative T_g at approximately -51 °C, which is consistent with literature values [35]. The literature [35,36] shows that when using DSC, NC has a positive T_g at about 53 – 56 °C. Upon analyzing the DSC recorded glass transition values for the PCL:NC blends, it becomes evident that the T_g transition shifts towards higher temperatures with an increase in NC content. This observation confirms the chemical stability and offers an opportunity to investigate the relationship between NC content and T_g transition temperatures further. The results can be attributed to the strong compatibility between PCL and NC, which is confirmed by the presence of a single T_g peak in the blends [35]. This single T_g peak occurs at a temperature between the T_g values of both pure polymers, which are -52 °C for PCL and 68 °C for NC. The T_g transition shifts to a higher temperature as the NC content increases. For PCL:NC 1:3 and 0:4 blends, the T_g transition is no longer observable.

The HNP formulations underwent DSC analysis to pinpoint the melting temperature of the composites in relation to the onset of chemical decomposition. This data is crucial for identifying the specific temperature range within which printing can be safely conducted.

By analyzing the thermal behavior of the composite propellants, illustrated in Fig. S11(a) and detailed in Table S5 from the supporting info file, it can be observed that in the cases where NC is present in the composition, the melting temperature onset of the polymeric matrix tends to decrease. At higher temperatures, in Fig. S11(b) and Table S6 from the supporting info file, two types of peaks are visible, the first one, endothermic, being attributed to RDX melting, and the second one, exothermic, being assigned to the decomposition of RDX. In Fig. S11(b), both the endothermic melting peak of RDX and the exothermic broad peak of the decomposition of RDX are observable for the 3D printable formulations labeled as HNP800020 and HNP570736. In the case of the formulation containing a higher NC content, denoted as HNP 701020, the melting point of RDX may approach the decomposition temperature range of NC. This proximity could complicate the differentiation of these events in the thermogram.

3.6. Safety and performance characteristics of the gun propellants

3.6.1. Impact and friction sensitivity of the gun propellant formulations

Considering the potential stress encountered during handling and transport, the developed energetic formulations were evaluated for their sensitivity to impact and friction. The 3D-printed gun propellant with the highest energetic content (HNP701020) was selected as the representative for evaluating the impact and friction sensitivity safety characteristics. The sensitivity characteristics with regard to friction and impact stimuli were examined in compliance with STANAG 4487 [31] and 4489 [30] using the apparatus detailed in the Materials and Methods section. Friction sensitivity analysis showed that both extruded and printed HNP701020 formulations are insensitive to the maximum applied friction force (360 N) on the BAM apparatus. Impact sensitivity tests showed that the impact

Table 2
Glass transition of the PCL:NC blends.

Blend PCL: NC	Onset/°C	End/°C	Half Cp Extrapol. /°C	Cp/(J·g ⁻¹ ·K ⁻¹)
4:0	-51.13	-46.74	-50.05	0.125
3:1	-48.99	-41.55	-45.79	0.443
2:1	-46.14	-35.93	-41.21	0.444
1:1	-36.27	-25.70	-32.29	0.324
1:2	-23.88	-14.77	-21.40	0.155
1:3	–	–	–	–
0:4	–	–	–	–

energy is directly influenced by the manufacturing process. Thus, extruded HNP701020 exhibited impact sensitiveness in the 20 – 21 J range, while the HNP701020 specimen that was 3D-printed possesses higher impact values in the interval of 23 – 24 J. The impact reactions recorded during the experiments are presented in Fig. S12 from the supporting info file.

3.6.2. Ballistic performances of the gun propellants

For the evaluation of the ballistic performances of the 3D-printed gun propellants, a closed vessel test was performed in the dedicated OZM apparatus (detail in the Methods section).

Table 3 summarizes the types of powders tested in the manometric bomb, along with their main characteristics, quantities used, and values obtained for maximal pressure, gas covolume, and propellant force. The pressure-times curves recorded are depicted in Fig. S14(b) from the supporting info file, and an exemplification of the setup for this test is illustrated in Figs. S3 and S13 from the supporting info file. To assess the influence of morphology modification caused by the additive manufacturing process on the performance of the HNP 701020 formulation, tests were carried out in the manometric bomb using granules (3 mm \times \varnothing 1.6 mm) obtained from a hot extruded filament and flakes obtained by cutting in 1.1 mm thin slices the 3D printed samples from Fig. 2. The data collected from the closed vessel test on HNP 701020 specimens (cylindrical granules obtained via hot extrusion and 3D printing) was used to determine the ballistic characteristics. The pressure corrections were made using the curve proposed by Muraour, following a procedure used in analogous previous studies [37].

The propellant force and the covolume (Table 3) were calculated using the maximum pressures measured for two different loading densities by employing the Noble and Able relationship, taking into account the contribution of the black powder primer (10 wt% of the propellant quantity). Noble and Abel's equation of state (Eq. (2)) describes the behavior of gases generated by the combustion of propellant in a sealed vessel:

$$P_{\max} = \frac{f \cdot \Delta}{1 - \alpha \cdot \Delta} \quad (2)$$

where P_{\max} is the maximum pressure, f is the propellant impetus (force constant), Δ is the loading density, and α is the propellant covolume. The values utilized for the black powder force and covolume are 274 MJ/kg and 0.55 cm³/g, respectively.

The HNP 701020 3D-printed flakes exhibit a slightly higher maximum pressure compared to the cylindrical granules produced from material subjected only to hot extrusion, but no significant differences were observed in terms of force and covolume calculated after the pressure correction.

For the coefficients of the burning rate law, $u = Ap^r$, the evolution of the time derivative of the burnt fraction $\frac{d\Psi}{dt}$ as functions of the burnt propellant fraction Ψ were considered, and the hypothesis that was used for two different loading densities implies that

Table 3
Closed vessel test.

Table 3 – Closed vessel test						
Propellant grain geometry	Diameter/ Thickness /mm	Quantity of propellant tested/g	Experimental maximal pressure/bar	Calculated maximal pressure/bar	Propellant force/ (kJ·kg ⁻¹)	Gas covolume/ (m ³ ·kg ⁻¹)
<i>HNP 800020</i>						
Porous spheric particles	∅ < 3	4	1085	1171	1032	0.893 × 10 ⁻³
Porous spheric particles	∅ < 3	6	1780	1853	–	–
Porous spheric particles	∅ > 3	6	1782	–	–	–
<i>HNP 570736</i>						
Cylindric (3D-printed)	∅ = 0.8	6	1191	–	–	–
<i>HNP 701020</i>						
Cylindric cold extruded	∅ = 1.6	6	1706	1860	1007	1.029 × 10 ⁻³
Cylindric cold extruded	∅ = 1.6	8	2504	2642	–	–
Cylindric cold extruded	∅ = 1.6	9	2983	3078	–	–
Cylindric (3D-printed)	∅ = 0.8	6	1834	–	–	–
Flakes ^b (3D-printed)	1.1	7	2033	2220	1005	1.013 × 10 ⁻³
Flakes ^b (3D-printed)	1.1	8	2556	2625	–	–
Flakes ^b (3D-printed)	1.1	9	2994	3057	–	–
Flakes ^a	–	6	1783	1890	1031	1.013 × 10 ⁻³
Flakes ^a	–	8	2590	2691	–	–

^a Flakes were obtained by crushing the cylindrical-shaped grains.

^b Flakes were obtained by cutting in thin slices the 3D-printed samples from Fig. 2.

the burning surface has the same evolution as a function of the burnt propellant fraction, following a procedure used in our previous studies [37,38]. Even if the HNP 701020 3D-printed flakes burn in a shorter time, as long as their thickness is only 1.1 mm compared to the cylindrical grains diameter of 1.6 mm, the specific burning rate is similar. The power index (ν) was 1.016, and the coefficient A was $0.661 \times 10^{-9} \text{ m/Pa}^{1.016} \text{ s}$ for the hot extruded cylinders and for the flakes obtained from 3D printed samples the power index (ν) was 1.024, and the coefficient A was $0.588 \times 10^{-9} \text{ m/Pa}^{1.024} \text{ s}$. The burning rate curves for determined A and ν coefficients are given in Fig. S14(e) and compared to JA2 specific curve.

All these results confirm that the 3D printing process, involving heating the gun propellant to 150 °C, does not adversely affect the

ballistic properties of the material.

In addition to the evaluation of HNP 701020 cylindrical propellant grains (room temperature extruded specimens), supplementary tests were conducted on specimens with a flake-like configuration obtained by crushing the cylindrical samples. These tests revealed a considerable reduction in burning times for the thin flake-type specimens, see Fig. S14(b) from the supporting info file, and a slight modification of the force and covolume values after pressure correction.

Due to the challenges experienced during the hot press extrusion process, the HNP800020 formulation was utilized to produce porous spherical granules directly in the form they were obtained from the shock-gel procedure. HNP800020 exhibited suboptimal extrusion behavior attributed to its structural inhomogeneity

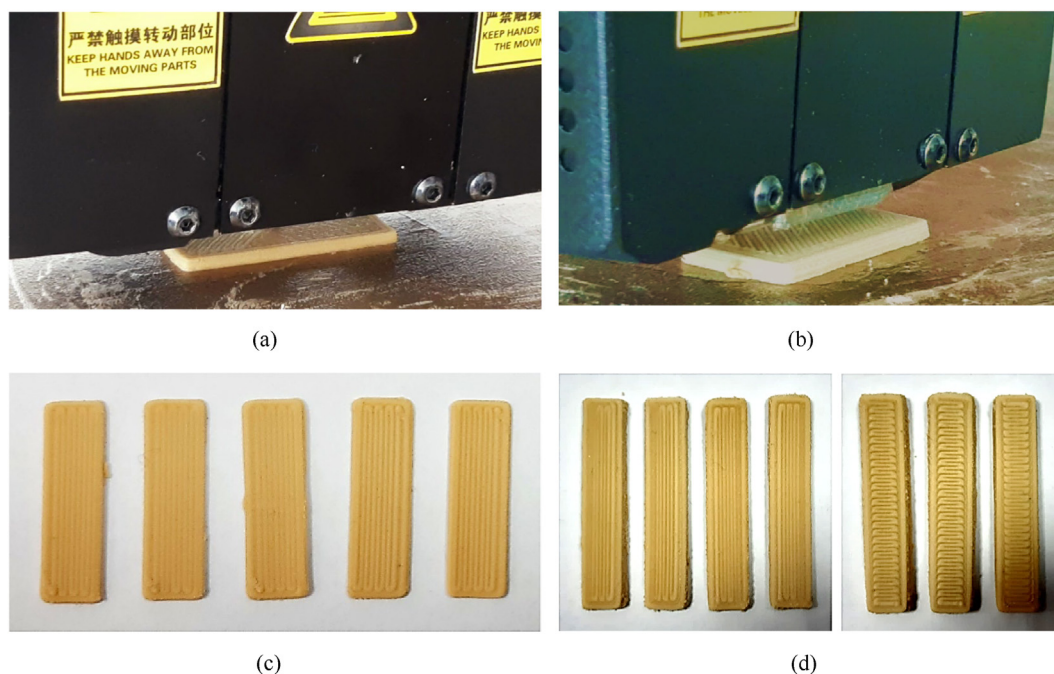


Fig. 2. Illustration of the FDM printing process and the 3D-printed materials obtained with Picoeate G5Pro FGF printer: (a) Printing the HNP570736 propellant; (b) Printing the HNP702010 propellant; (c) HNP570736 propellant printed in the form of long stripes; (d) HNP701020 propellant printed with two orientations.

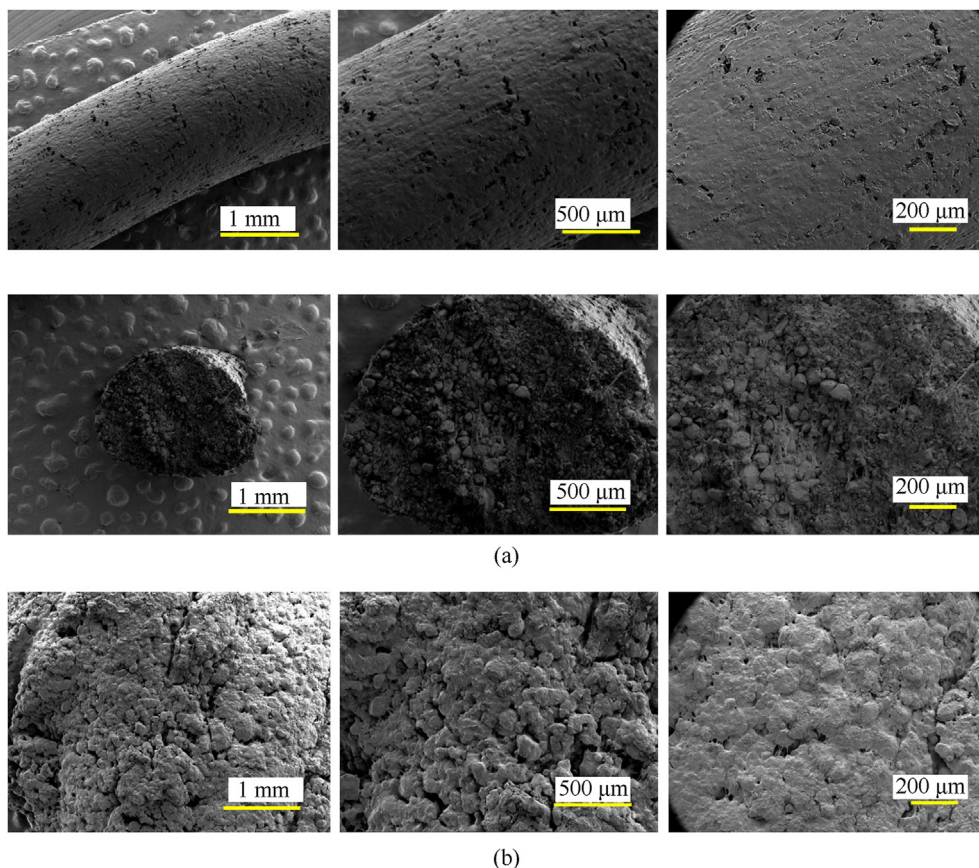


Fig. 3. SEM images for HNP701020 propellant formulation:(a) The extruded filament HNP701020; (b) 3D printed HNP701020 propellant formulation.

resulting from the absence of nitrocellulose, as elucidated in subsection 3.2. The porous structure of HNP800020 (Fig. S6(b)), as also evidenced by the imperceptible variations in the curves obtained from tests conducted at identical loading densities but with granules of different sizes (Table 3), hindered the determination of the burning speed coefficients. The closed vessel test for the HNP 570736 formulation involved utilizing 6 g of cylindrical granules obtained by cutting the thread produced through additive manufacturing ($3 \text{ mm} \times \varnothing 1.6 \text{ mm}$). The test results indicated a significantly lower maximum pressure of only 1191 bar compared to other formulations. Moreover, a substantial amount of solid residue was noted in the bomb chamber. Consequently, it was

determined that the HNP 570736 formulation was unsuitable for ballistic applications. As a result, the pressure adjustments needed to quantify the heat transfer to the walls of the manometric bomb chamber and the necessary calculations to determine the ballistic characteristics were omitted.

3.7. Mechanical properties of the 3D-printed gun propellant

While the mechanical properties of gun propellants may not hold the same level of critical importance as those of rocket propellants, gaining a comprehensive understanding and optimizing these properties can significantly contribute to enhancing safety, reliability, and overall performance. While gun propellants may receive less focus on their mechanical properties than rocket propellants do, these attributes are nonetheless important. The mechanical integrity of the propellant plays a vital role in its manufacturing, handling, storage, and performance under various conditions. Characteristics such as brittleness and ductility significantly affect the propellant's response to stress, which is essential during the manufacturing process and for ensuring the reliability of the final product. Furthermore, these mechanical qualities influence the uniformity of the propellant grain, which in turn affects the consistency of the burn rate and overall ballistic performance.

Upon investigating the chemical stability, compatibility, thermal properties, safety, and performance of the composite propellants, and at the same time correlating data collected with the properties of individual components and relevant PCL-NC blends, the final step of this study implied conducting mechanical analyses (dynamic mechanical analysis, shear testing, uniaxial tensile testing, and 3-point bending characterization) exclusively for the

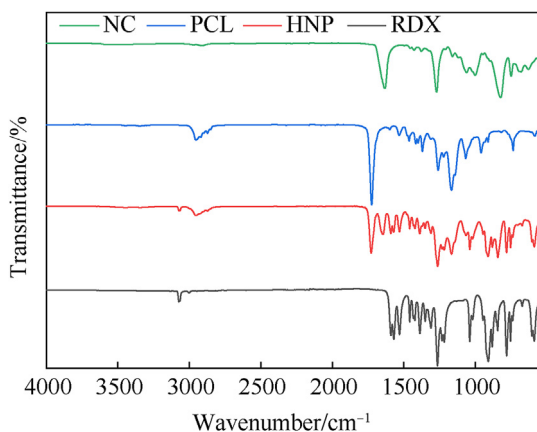


Fig. 4. Comparative FT-IR spectra for HNP701020, NC, PCL, and RDX.

HNP701020 formulation obtained via additive manufacturing, as it exhibited the most favorable characteristics for the design of an FDM 3D-printed gun propellant. In the final round of investigations, a DMA instrument was used to analyze the mechanical strength of specimens produced through the FDM printing technique. These mechanical tests aimed to assess the ability of the 3D-printed specimens to withstand different types of forces encountered throughout their lifecycle.

3.7.1. DMA single cantilever temperature ramp scan

To investigate the viscoelastic properties of the 3D-printed gun propellants, a single-cantilever setup (Fig. S15 from the supporting info file) was employed for the DMA analysis in the temperature range $-80\text{ }^{\circ}\text{C}$ to $+25\text{ }^{\circ}\text{C}$, and the results obtained are illustrated in Fig. 5.

DMA analysis reveals various forms of transitions and relaxations that are associated with the structural and morphological characteristics of the 3D-printed specimens. Based on Fig. 5, in the glassy-state region, the storage modulus of the 3D-printed HNP701020 sample slightly surpasses the storage modulus obtained for the 3D-printed PCL sample, probably due to the presence of a higher solid content and the likely formation of additional hydrogen bonds between the components. As the temperature increases, the interactions between the components in the propellant weaken [39], resulting in a gradual but more noticeable decrease in the storage modulus of HNP701020 with increasing temperature. Additionally, the presence of NC, which acts as a plasticizing agent, may also influence this behavior of the 3D-printed HNP701020 sample at higher temperatures. The loss modulus is associated with the mechanical response resulting from the thermal effects applied on the molecular chains of the binder during its viscosity deformation. An increase in temperature can improve the mobility of these molecular chains, thereby increasing the probability of viscosity deformation. As outlined in STANAG 4540 [40], the maximum values of the loss modulus E'' for propellants can serve as indicative of their glass transition temperatures. DMA offers the significant benefit of heightened sensitivity to relaxations occurring at or below the glass transition temperature (T_g) [35]. Consequently, this technique has been utilized to determine T_g values that may not be identifiable through Differential Scanning Calorimetry (DSC) [34]. A variation of up to $20\text{ }^{\circ}\text{C}$ in the T_g values obtained from Differential Scanning Calorimetry (DSC) and Dynamic Mechanical Analysis (DMA) is considered acceptable,

attributable to the fundamental principles underlying each method [35]. The glass transition temperature is commonly used to evaluate the miscibility of polymers, making it an essential tool for the characterization of polymer blends [35]. Blends that display a singular glass transition temperature that lies between the T_g values of the constituent polymers are considered to demonstrate a substantial level of miscibility [35]. According to DMA single-cantilever analysis, the highest recorded value of the loss modulus for the 3D-printed specimen containing only PCL shows that its glass transition temperature is located around $-40\text{ }^{\circ}\text{C}$, while for the 3D-printed HNP701020 sample, two E'' peaks were observed at $-50\text{ }^{\circ}\text{C}$ and $-8\text{ }^{\circ}\text{C}$, indicating a phase segregation of the hard (RDX crystals) and soft components (PCL: NC blend) of the composite propellant. The ratio of E'' to E' yields $\tan \delta$, which serves as the mechanical damping factor [35]. $\tan \delta$ reflects the efficiency of the material in dissipating energy during molecular rearrangements. The loss factor ($\tan \delta$) illustrates the fundamental characteristics of the propellant at the molecular level through the α and β relaxations [39]. Consequently, the two $\tan \delta$ values observed for the 3D-printed HNP701020 sample could also be elucidated by the presence of both α and β relaxations. The α relaxation arises from the motion of the primary molecular chain within the propellant. In contrast, the β relaxation could be attributed to the movement of interconnected chains, including short chains, branched chains, and other chain structures present in the propellant [39]. Usually, the higher temperature peak corresponds to a glass transition, while the lower temperature peak may be attributed to a secondary relaxation [34].

3.7.2. Frequency-dependent evaluation of viscoelastic properties utilizing a double sandwich shear geometry

The viscoelastic properties of the 3D-printed specimens were also evaluated using a double sandwich shear geometry (Fig. S16(a) from the supporting info file), and the results are illustrated in Fig. 6. For this type of analysis, analogous to the information presented above for a single-cantilever DMA test, the viscoelastic properties of materials [41] can be defined by two key parameters: the storage modulus (G') and the loss modulus (G''). The storage modulus reflects the energy retained through elastic deformation. In contrast, the loss modulus pertains to the energy lost due to viscous deformation. The ratio of the loss modulus to the storage modulus ($G''/G' = \tan \delta$), known as the damping factor, serves as an indicator of the mechanical energy loss in materials. Some characteristics of viscoelastic materials regularly exhibit a dependence on time (frequency) [42]. Analyzing the relationship between shear moduli and frequency provides valuable information regarding the damping characteristics of the 3D-printed specimens, which elucidates the dissipation of mechanical energy through internal motions, as represented by the loss modulus and the $\tan \delta$ [42]. A comparative assessment of the mechanical characteristics of PCL specimens in conjunction with the 3D-printed HNP composite indicates that the latter demonstrates higher values of both storage and loss modulus in the 10^{-1} – 10^1 Hz range, suggesting that the HNP propellant possesses a slightly higher capacity for the storage and dissipation of mechanical energy. This quality can be beneficial for gun propellants, which may encounter diverse mechanical stresses during their lifecycle. However, at higher frequencies (in the 10^1 – 10^2 Hz range), the decrease of storage modulus of the 3D-printed HNP formulation suggests a shift towards a more viscous behavior in the material. In contrast, the neat PCL sample seems to demonstrate a nearly independent relationship with frequency.

3.7.3. Uniaxial tensile test for the 3D-printed materials

Uniaxial tensile testing (Fig. S16(b) from the supporting info file) provides essential insights into the performance and reliability of

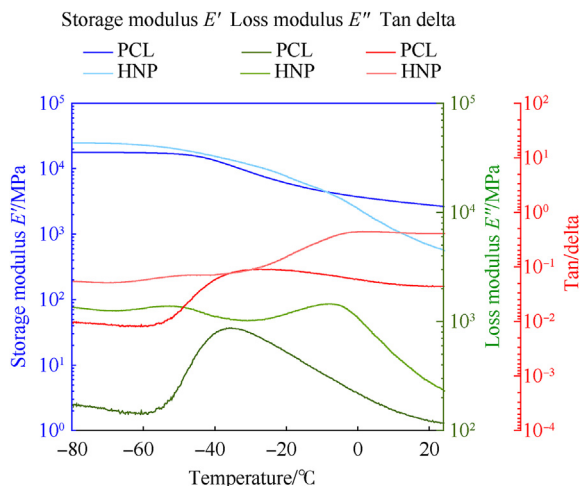


Fig. 5. Storage modulus, loss modulus, and $\tan(\delta)$ for the 3D-printed propellant HNP701020 and comparison with 3D-printed PCL specimen.

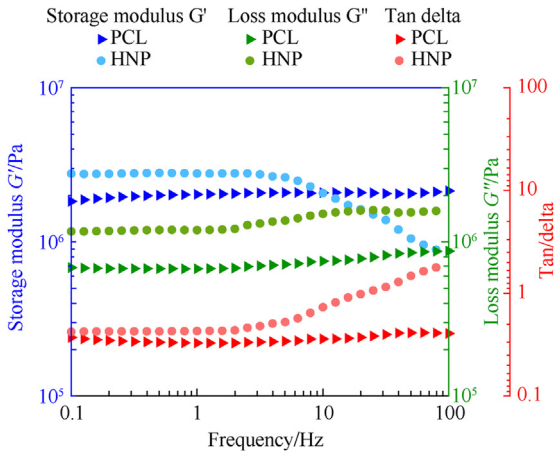


Fig. 6. Results obtained for double sandwich shear geometry.

gun propellants produced through fused deposition modeling (FDM) by evaluating the mechanical properties such as tensile strength, elongation at break, and elasticity while offering an overview of the interlayer strength of the 3D printed superposed layers. Understanding interlayer adhesion is crucial for ensuring the safety and effectiveness of gun propellants, as strong bonds can help reduce the risks of delamination and failure during use. Data obtained from tensile testing is vital for optimizing binder formulations in composite materials since binders have a significant impact on mechanical properties through their adhesion to RDX crystals. As a result, uniaxial tensile testing is essential for selecting appropriate binder systems and advancing composite materials that meet modern ammunition standards, ultimately enhancing both performance and safety in FDM-printed gun propellants. Fig. 7 illustrates a comparative graph of the tensile test results obtained for PCL and HNP701020 specimens. As can be observed from this graph, the mechanical behavior of the 3D-printed specimens is influenced by the composition of the sample tested. PCL demonstrates a tendency towards brittleness, characterized by a restricted strain and a tendency to fracture abruptly. In contrast, HNP specimens display more ductile properties, allowing them to achieve greater strain values prior to failure. This suggests that HNP materials can undergo considerable plastic deformation before ultimately breaking.

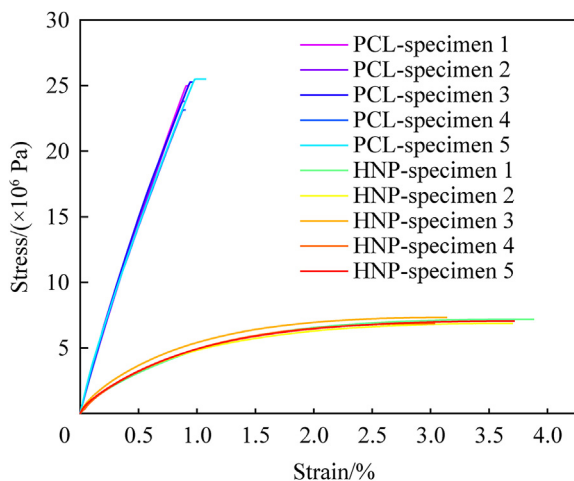


Fig. 7. Stress-strain plots for tensile test of the 3D-printed materials HNP701020.

In composite materials, the presence of large-scale phase segregation can result in poor mechanical properties due to the existence of large domains with weak interfacial bonding. Conversely, a compatible formulation demonstrates a higher degree of interfacial bonding, leading to mechanical properties that reflect an average between the constituents [34]. The mean maximal stress values being approximately 2.5 MPa and 0.69 MPa obtained for neat PCL and HNP, respectively, indicate good compatibility between the components and an appropriate mechanical resistance of the 3D-printed propellant, comparable with literature data for analogous propellants [6,12,43].

The last type of DMA mechanical test performed was the three-point bending test, which was executed in oscillation mode (amplitude scanning, details in *Materials and methods* section and Figs. S17(a) and S17(b) from the *supporting info file*). The results obtained are comparatively illustrated below in Figs. S17(d) and S17(e).

For all the samples tested, the crack propagation nearly divided the core of the 3D-printed specimen into two separate parts, as can be observed from Figs. S17(c) from the *supporting info file*. As can be observed from Figs. S17(d) and S17(e), HNP formulations exhibited a reduction in flexural resistance as the oscillation amplitude increased more than 0.07 mm. This behavior is attributed to their superior malleability compared to unmodified PCL specimens, which display increased stiffness and sustain higher flexural resistance over a wider range of oscillation amplitudes during flexural resistance testing. HNP formulations possess greater malleability, as was also demonstrated through tensile assessments, but they may compromise some aspects of structural integrity under specific loading conditions. Although HNP formulations may be beneficial for applications necessitating flexibility and adaptability, it is essential to maintain a careful equilibrium between flexibility and strength to ensure the performance and endurance of gun propellants.

3.7.4. Compressive tests

HNP 701020 was the only material submitted to uniaxial compression tests. In the static tests the universal testing machine was set to a crosshead speed of 1 mm/min. The raw data obtained (force vs. displacement) were processed with classical mathematical relations, in which the assumptions of the sample volume invariability and the preservation of its hexahedral shape were taken into account, to draw the true tension vs. true strain diagram for large values of the strain, Fig. 8. The elastic modulus of tested samples is 30 MPa and the maximum stress value spreads between 2.58 MPa and 2.72 MPa. All the tested specimens were subjected to very large deformations without an obvious breaking point, even if the post-test analysis highlighted the existence of cracks in the samples. At the same time, the calculated curves show that after reaching the maximum tension, there is a portion where the material shows a slightly strain-softening, up to a true strain of 0.4–0.5, after which the strain-hardening phenomenon occurs.

In the dynamic tests the projectile initial velocities, between 3.7 m/s and 5.7 m/s, were calculated based on the images acquired by the high speed camera used at 25000 fps. The data recorded by accelerometer have required an initial filtering. The resulting values were multiplied by the projectile mass in order to calculate the force that acts on the sample. Using the same data and the kinematic equations were calculated the projectile velocity reduction and the projectile displacement. Knowing the evolution of the projectile velocity also allowed the calculation of the strain rate, which starts from initial values of 550–750 s⁻¹ and remains relatively constant during most of the compression process, Fig. S18(a). The true stress and true strain of the sample σ - ϵ were calculated using the same assumptions as in the case of the static tests. Even if

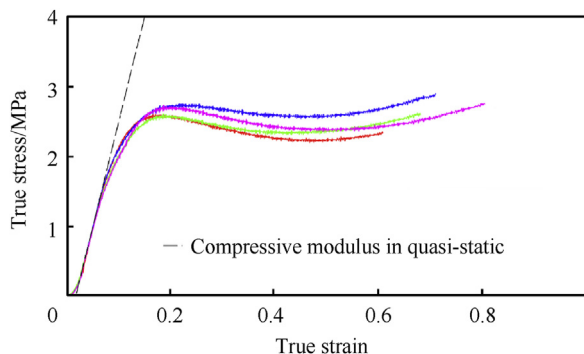


Fig. 8. Static true stress-strain curves.

a filter was used for the raw data, the true stress vs. true strain curves show oscillations, whose amplitudes increase in the second part of the recording, which is why these curves are shown truncated in Fig. 9 for a better visualization of the data. A complete curve, with values of true strain close to 1, is presented in Fig. S18(b). Contrary to what was observed in the static tests, the strain-hardening phenomenon is observed right from the beginning, after the yielding point is exceeded. The elastic modulus of tested samples is 0.45 GPa and the maximum stress value in first oscillation spreads between 27 MPa and 30 MPa. The values σ - ϵ measured in the dynamic tests confirm the results obtained with DMA, namely that the propellant made by 3D printing is a highly viscous material. The analysis of the recorded images showed that the macrocracks appear late, after the specimen reaches true stress values of 0.5, Fig. S19. At the same time, the post-test measurements of the samples showed much lower values of the residual true strain than the maximum attained, Fig. S19. The existence of a

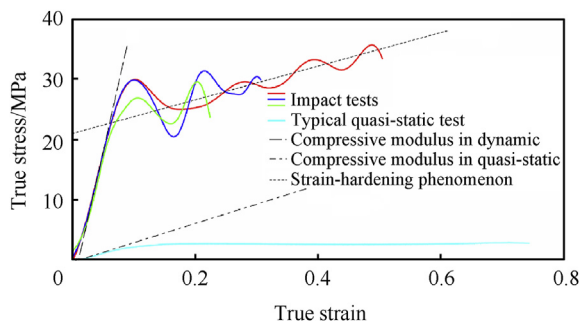


Fig. 9. Static vs. dynamic true stress-strain curves.

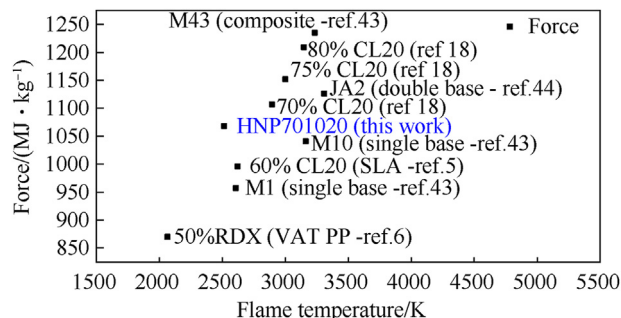


Fig. 10. Comparative plot on ballistic performance.

considerable difference between the minimum height of the samples reached during the test and their final height after removing the load is justified by the hyperelasticity of the tested material.

3.8. Comparative evaluation of the current study achievements

We have achieved a breakthrough by exceeding the standard limit of 60 wt% energetic solids loading in gun propellant formulations created using stereolithography or light-curing 3D printing technologies. In terms of ballistic energy, the HNP 701020 developed 1068 MJ/kg with a calculated adiabatic flame temperature of 2481 K, while previous work on 3D printed propellants [3,8] reported ballistic energy less than 1000 MJ/kg and a higher, undesirable, flame temperature [8]. In comparison with conventional propellants [44,45], the HNP701020 provides a reasonable amount of ballistic energy (typical for double-base propellants), while the flame temperature is kept under 2600K, like in low-energy, cool single-base propellants. Table 4 and the comparative plot illustrated in Fig. 10 provide an overview of current work achievements focusing on force and flame temperature as key parameters in evaluating ballistic performance.

From the mechanical point of view, the HNP701020 formulation is softer than JA2 propellant when is deform quasistatic (for a strain rate of 0.01 s⁻¹ the JA2 compression modulus is reported to be 190 MPa with a yield stress of 4.49 MPa [47]), but for dynamic loadings, the HNP701020 formulation has a consistently higher flow stress compared to JA2, even if the modulus of elasticity remains lower (for strain rates between 100 and 250 s⁻¹, the JA2 compression modulus is reported to be in the interval 0.56–0.79 GPa [47–49] and according to the dedicated calculation formula [50] the flow stress of JA2 is approximately 16 MPa for the strain rates achieved in our dynamic tests).

Table 4 Comparative evaluation of the current study achievements.

Energetic solids loading and their theoretical density	Technique employed	Advantages	Disadvantages	Refs.
50% RDX ($\rho = 1.806 \text{ g/cm}^3$)	Stereolithography (SLA)	Adequate mechanical properties	High pressure exponent Low linear burning rate Low energy	[6]
50% RDX ($\rho = 1.806 \text{ g/cm}^3$)	light-curing 3D printing	Good chemical stability	High pressure exponent Low energy	[7]
60% CL20 (2.04 g/cm^3)	Stereolithography (SLA)	Acceptable performance	Low burning rate High content of soot products	[8]
70–80% CL20 (2.04 g/cm^3)	Light curing extrusion printing	High energetic content	Very high-pressure exponent	[18]
70% RDX ($\rho = 1.806 \text{ g/cm}^3$) 10% NC ($\rho = 1.655 \text{ g/cm}^3$)	FDM	High energetic content. Pressure exponent $\cong 1$ Burning rate comparable with JA2 [46]	Tendency to fuse when parts are left in contact without proper surface treatment (graphite addition)	This study

4. Conclusions

This study presents an efficient strategy for 3D-printing gun propellants with high energetic solid content using the Fused Deposition Modeling (FDM) approach. The application of FDM additive manufacturing technology to produce gun propellants marks a significant advancement, representing a new and innovative use in this field. Three formulations were identified utilizing EXPLO5™, of which two demonstrated suitability for 3D printing. The formulation HNP701020 (70 wt% RDX, 10 wt% NC, 20 wt% PCL), exhibited optimal characteristics, including reduced roughness and sufficient mechanical strength for ballistic applications. The formulations were prepared by blending NC and PCL solutions with RDX powder. The shock-gel procedure effectively removed the solvent, and hot press extrusion was used to generate the feedstock for FDM printing. SEM analysis indicated that the filament from HNP701020 demonstrated optimal NC content, exhibiting lower roughness compared to the other formulations. The HFC test results showed that nitrocellulose (NC) is the primary heat-generating substance, resulting from the autocatalytic de-nitration of cellulose in the absence of a chemical stabilizer. DSC analysis indicated that the inclusion of NC lowers the onset melting temperature of the polymeric matrix. Furthermore, friction sensitivity tests revealed that both extruded and printed formulations are insensitive to a maximum applied friction force of 360 N. Impact sensitivity tests indicated for the extruded HNP701020 a 20–21 J range, while 3D-printed HNP701020 was 23–24 J. The enclosed vessel test confirmed that HNP701020 is suitable for gun propellant use. Mechanical evaluations, including dynamic mechanical analysis, shear testing, uniaxial tensile testing, three-point bending tests, and uniaxial compression static and dynamic tests, indicated that the HNP701020 formulation possesses sufficient mechanical strength for ballistic applications and the capability to store and dissipate mechanical energy effectively.

The results of this study regarding FDM 3D printing of gun propellants carry substantial practical implications for defense and security, justified by the attainment of enhancements in both performance and manufacturability of energetic thermoplastic composites.

CRediT authorship contribution statement

Marin Alexandru: Writing – original draft, Software, Investigation, Data curation, Conceptualization. **Ovidiu George Iorga:** Writing – review & editing, Writing – original draft, Supervision, Resources, Project administration, Investigation, Funding acquisition, Conceptualization. **Gabriela Toader:** Writing – review & editing, Writing – original draft, Validation, Supervision, Methodology, Investigation. **Cristiana Epure:** Visualization, Software, Methodology, Investigation, Data curation. **Mihail Munteanu:** Software, Methodology, Investigation, Data curation. **Adrian Nicolae Rotariu:** Writing – original draft, Validation, Software, Resources, Methodology, Investigation, Data curation. **Marius Marmureanu:** Visualization, Resources, Methodology, Investigation, Conceptualization. **Gabriel Flavius Noja:** Writing – original draft, Software, Investigation, Data curation. **Aurel Diacon:** Writing – review & editing, Visualization, Validation, Investigation, Formal analysis. **Tudor Viorel Tiganescu:** Writing – original draft, Investigation, Funding acquisition, Formal analysis. **Florin Marian Dirloman:** Writing – original draft, Investigation, Formal analysis, Data curation.

Data availability

The data that support the findings of this study are available on

request from the corresponding author.

Declaration of competing interest

The authors declare that they have no known competing financial interests or personal relationships that could have appeared to influence the work reported in this paper.

Acknowledgments

This work was supported by a grant from the Ministry of Research, Innovation and Digitization, UEFISCDI, Grant Nos. PN-III-P2-2.1-PED-2021-1890, PN-IV-P6-6.3-SOL-2024-2-0254 and PN-IV-P7-7.1-PTE-2024-0517, within PNCDI IV.

Appendix A. Supplementary data

Supplementary data to this article can be found online at <https://doi.org/10.1016/j.dt.2025.02.024>.

References

- [1] Muravyev NV, Monogarov KA, Schaller U, Fomenkov IV, Pivkina AN. Progress in additive manufacturing of energetic materials: creating the reactive microstructures with high potential of applications. *Propellants, Explos Pyrotech* 2019;44(8):941–69. <https://doi.org/10.1002/prep.201900060>.
- [2] Deng Y, Wu X, Deng P, Guan F, Ren H. Fabrication of energetic composites with 91% solid content by 3D direct writing. *Micromachines* 2021;12(10):1160.
- [3] Cano-Vicent A, et al. Fused deposition modelling: current status, methodology, applications and future prospects. *Addit Manuf* 2021;11/01/2021;47:102378. <https://doi.org/10.1016/j.addma.2021.102378>.
- [4] Song S, Ren Q, Tang M, Shi J, Wang J. A study on ultra-low-pressure ratio technology on the basis of 3D-printed propellant for a solid rocket motor. *Aerospace* 2023;10(10):862. <https://doi.org/10.3390/aerospace10100862>.
- [5] Kristiawan RB, Imaduddin F, Ariawan D, Ubaidillah, and Z. Arifin, "A review on the fused deposition modeling (FDM) 3D printing: filament processing, materials, and printing parameters.", *Open Eng* 2021;11(1):639–49. <https://doi.org/10.1515/eng-2021-0063>.
- [6] Yang W, Hu R, Zheng L, Yan G, Yan W. Fabrication and investigation of 3D-printed gun propellants. *Mater Des* 2020;07/01/2020;192:108761. <https://doi.org/10.1016/j.matdes.2020.108761>.
- [7] Straathof MH, van Driel CA, van Lingen JNJ, Ingenhuth BLJ, ten Cate AT, Maalderink HH. Development of propellant compositions for vat photopolymerization additive manufacturing. *Propellants, Explos Pyrotech* 2020;45(1):36–52. <https://doi.org/10.1002/prep.201900176>.
- [8] Li M, Yang W, Xu M, Hu R, Zheng L. Study of photocurable energetic resin based propellants fabricated by 3D printing. *Mater Des* 2021;09/01/2021;207:109891. <https://doi.org/10.1016/j.matdes.2021.109891>.
- [9] Whyte DJ, Doeven EH, Sutti A, Kouzani AZ, Adams SD. Volumetric additive manufacturing: a new frontier in layer-less 3D printing. *Addit Manuf* 2024/03/25/2024;84:104094. <https://doi.org/10.1016/j.addma.2024.104094>.
- [10] Kirby L, Lawrence A, Udaykumar HS, Sippel T, Song X. Pressure-assisted binder jet additive manufacturing of solid propellants. *Addit Manuf* 2023;77:103808. <https://doi.org/10.1016/j.addma.2023.103808>.
- [11] Mostafaei A, et al. Binder jet 3D printing—process parameters, materials, properties, modeling, and challenges. *Prog Mater Sci* 2021;06/01/2021;119:100707. <https://doi.org/10.1016/j.pmatsci.2020.100707>.
- [12] Tan B, et al. 3D printing for explosives and propellants applications. *Additive Manufacturing Frontiers* 2024/09/01/2024;3(3):200151. <https://doi.org/10.1016/j.amf.2024.200151>.
- [13] Zong H, et al. Rheological and printability evaluation of melt-cast explosives for fused deposition modeling (FDM) 3D printing. *FirePhysChem* 2024/03/01/2024;4(1):34–41. <https://doi.org/10.1016/j.fpc.2023.05.007>.
- [14] Zhang J-c, et al. Three-dimensional printing of energetic materials: a review. *Energetic Materials Frontiers* 2022/06/01/2022;3(2):97–108. <https://doi.org/10.1016/j.enmf.2022.04.001>.
- [15] Al Rashid A, Ahmed W, Khalid MY, Koç M. Vat photopolymerization of polymers and polymer composites: processes and applications. *Addit Manuf* 2021/11/01/2021;47:102279. <https://doi.org/10.1016/j.addma.2021.102279>.
- [16] Gajbhiye TS, et al. Polymer composite additive manufacturing: applications, challenges and opportunities. *Mater Today Proc* 2024/06/18/2024. <https://doi.org/10.1016/j.matpr.2024.06.013>.
- [17] Stec D, Wilson A, Fuchs BE, Mehta N, Cook P. US8636861B1 - high explosive fills for MEMS devices. 2014.
- [18] Gao Y, Yang W, Hu R, Zhou J, Zhang Y. Validation of CL-20-based propellant formulations for photopolymerization 3D printing. *Propellants, Explos Pyrotech* 2021;46(12):1844–8. <https://doi.org/10.1002/prep.202100196>.

- [19] Wang M, Jin G, He W, Nan F. 3D printing of gun propellants based on laminated object manufacturing. *Mater Manuf Process* 2022;37(11):1246–56. <https://doi.org/10.1080/10426914.2022.2072884>.
- [20] Kudryashova O, Lerner M, Vorozhtsov A, Sokolov S, Promakhov V. Review of the problems of additive manufacturing of nanostructured high-energy materials. *Materials* 2021;14(23):7394. <https://doi.org/10.3390/ma14237394>.
- [21] Reyes RL, Ghim M-S, Kang N-U, Park J-W, Gwak S-J, Cho Y-S. Development and assessment of modified-honeycomb-structure scaffold for bone tissue engineering. *Addit Manuf* 2022;54:102740. <https://doi.org/10.1016/j.addma.2022.102740>.
- [22] Ahn J-H, et al. "3D-printed biodegradable composite scaffolds with significantly enhanced mechanical properties via the combination of binder jetting and capillary rise infiltration process,". *Addit Manuf* 2021;41:101988. <https://doi.org/10.1016/j.addma.2021.101988>, 2021/05/01/.
- [23] Arif ZU, Khalid MY, Noroozi R, Sadeghianmaryan A, Jalalvand M, Hossain M. Recent advances in 3D-printed polylactide and polycaprolactone-based biomaterials for tissue engineering applications. *Int J Biol Macromol* 2022/10/01/2022;218:930–68. <https://doi.org/10.1016/j.ijbiomac.2022.07.140>.
- [24] Yang X, Wang Y, Zhou Y, Chen J, Wan Q. The application of polycaprolactone in three-dimensional printing scaffolds for bone tissue engineering. *Polymers* 2021;13(16):2754. <https://doi.org/10.3390/polym13162754>.
- [25] Jiba Z, Focke WW, Kalombo L, Madito MJ. Coating processes towards selective laser sintering of energetic material composites. *Defence Technology* 2020/04/01/2020;16(2):316–24. <https://doi.org/10.1016/j.dt.2019.05.013>.
- [26] Haung C, Yeh T, Perng H. Thermal behavior of propellants containing polycaprolactone as binder. *Kogyo Kayaku (Journal of the Industrial Explosives Society)* 1993;54(5). Japan.
- [27] Man-man L, Ruo-heng W, Yu-chen G, Wei-tao Y, Rui H, Qiong-lin W. The influence of CL-20 particle size on the thermal decomposition and combustion performances of 3D printed photocurable propellants. *Chin J Explos Propellants* 2023;46(4). <https://doi.org/10.14077/j.issn.1007-7812.202301005>.
- [28] Sućeska M. "Calculation of the detonation properties of C H N O explosives,". *Propellants, Explos Pyrotech* 1991;16(4):197–202. <https://doi.org/10.1002/prep.19910160409>.
- [29] Stanag 4582 - explosives, nitrocellulose based propellants, stability test procedure and requirements using heat flow calorimetry. N. S. Agency; 2007.
- [30] STANAG 4489 - Explosives. Impact sensitivity tests, N. S. Agency. 1999.
- [31] STANAG 4487 - Explosives. Friction sensitivity tests, N. S. Agency. 2002.
- [32] STANAG. 4147 - Chemical compatibility of ammunition components with explosives (non-nuclear applications). Edition 2, 2001.
- [33] Nguyen TT, Phan DN, Nguyen DC, Do VT, Bach LG. The chemical compatibility and adhesion of energetic materials with several polymers and binders: an experimental study. *Polymers* 2018;10(12):1396. <https://doi.org/10.3390/polym10121396>.
- [34] Hubbell DS, Cooper SL. The physical properties and morphology of poly-ε-caprolactone polymer blends. *J Appl Polym Sci* 1977;21(11):3035–61. <https://doi.org/10.1002/app.1977.070211117>.
- [35] de Paula AC, Uliana F, da Silva Filho EA, Soares K, Luz PP. Use of DMA-material pocket to determine the glass transition temperature of nitrocellulose blends in film form. *Carbohydr Polym* 2019/12/15/2019;226:115288. <https://doi.org/10.1016/j.carbpol.2019.115288>.
- [36] Mark JE. *Polymer data handbook*. second ed. Oxford University Press; 2009.
- [37] Dirloman F-M, Rotariu A-N, Rotariu T, Noja G-F, Ginghină R-E, Zvinco N-D. Ballistic and thermal characterisation of greener composite solid propellants based on phase stabilized ammonium nitrate. *Case Stud Therm Eng* 2024/02/01/2024;54:103987. <https://doi.org/10.1016/j.csite.2024.103987>.
- [38] Noja GF, Rotariu AN, Mărmureanu MI, Malciu A, Pulpea BG, Dîrloman FM. "Theoretical and experimental research on gun propellant burning,". *Problemy Mechatroniki: uzbrojenie, lotnictwo, inżynieria bezpieczeństwa* 2022;13(50):9–22. <https://doi.org/10.5604/01.3001.0016.1453>.
- [39] Yuan S, Zhang B, Wen X, Chen K, Jiang S, Luo Y. Investigation on mechanical and thermal properties of HTPE/PCL propellant for wide temperature range use. *J Therm Anal Calorim* 2022/04/01 2022;147(8):4971–82. <https://doi.org/10.1007/s10973-021-10708-3>.
- [40] STANAG 4540 - Explosives. Procedures for dynamic mechanical analysis (DMA) and determination of glass transition temperature. N. S. Agency; 2002.
- [41] Luo Y, et al. Process fundamentals and quality investigation in extrusion 3D printing of shear thinning materials: extrusion process based on Nishihara model. *Int J Adv Des Manuf Technol* 2023/01/01 2023;124(1):245–64. <https://doi.org/10.1007/s00170-022-10506-7>.
- [42] Dirloman FM, et al. "Novel polyurethanes based on recycled polyethylene terephthalate: synthesis, characterization, and formulation of binders for environmentally responsible rocket propellants,". *Polymers* 2021;13(21):28. <https://doi.org/10.3390/polym13213828> (in English).
- [43] Wilkinson PJ. Evaluation of novel propellants manufactured from commercially available Thermoplastic Elastomers (TPE) using resonant acoustic mixing. Cranfield University; 2019.
- [44] Miller MS. Thermophysical properties of six solid gun propellants. In: ARLTR-1322. US Army Research Laboratory; 1997.
- [45] Manning TG, Leone J, Zebregs M, Ramlal DR, van Driel CA. Definition of a JA-2 equivalent propellant to be produced by continuous solventless extrusion. *J Appl Mech* 2013;80(3):031405. <https://doi.org/10.1115/1.4023315>.
- [46] Derk G. High-pressure burning-rates of JA2 and nitromethane propellants. 2019.
- [47] Gazonas G. The mechanical response of M30, XM39, and JA2 propellants at strain rates from 10-2 to 250 sec-1. In: BRL-TR-3181. MD: Army Research Laboratory Aberdeen; 1991.
- [48] Leadore MG. Mechanical properties of aerojet, thiokol, and JA2 high-energy gun propellants at 1.5 m/s deformation rate. ARL-TR-2654, US Army Research Laboratory; 2002.
- [49] Howard SL, Leadore MG, Newberry JE. High-rate mechanical properties of JA2 propellant at temperatures from -50 to 80 C. In: ARL-MR-0894. US Army Research Laboratory; 2015.
- [50] Trębiński R, Janiszewski J, Leciejewski Z, Surma Z, Kamińska K. On influence of mechanical properties of gun propellants on their ballistic characteristics determined in closed vessel tests. *Materials* 2020;13(14):3243. <https://doi.org/10.3390/ma13143243>.